



Investigation of satellite vertical sensitivity on long-term retrieved lower tropospheric ozone trends

Richard J Pope, Fiona M O'Connor, Mohit Dalvi, Brian J Kerridge, Richard Siddans, Barry G Latter, Brice Barret, Eric Le Flochmoen, Anne Boynard, Martyn P Chipperfield, et al.

► To cite this version:

Richard J Pope, Fiona M O'Connor, Mohit Dalvi, Brian J Kerridge, Richard Siddans, et al.. Investigation of satellite vertical sensitivity on long-term retrieved lower tropospheric ozone trends. Atmospheric Chemistry and Physics Discussions, In press, 10.5194/egusphere-2023-3109 . insu-04372824

HAL Id: insu-04372824

<https://insu.hal.science/insu-04372824>

Submitted on 4 Jan 2024

HAL is a multi-disciplinary open access archive for the deposit and dissemination of scientific research documents, whether they are published or not. The documents may come from teaching and research institutions in France or abroad, or from public or private research centers.

L'archive ouverte pluridisciplinaire **HAL**, est destinée au dépôt et à la diffusion de documents scientifiques de niveau recherche, publiés ou non, émanant des établissements d'enseignement et de recherche français ou étrangers, des laboratoires publics ou privés.



Richard J. Pope^{1,2}, Fiona M. O'Connor^{3,4}, Mohit Dalvi³, Brian J. Kerridge^{5,6}, Richard Siddans^{5,6}, Barry G. Latter^{5,6}, Brice Barret⁷, Eric Le Flochmoen⁷, Anne Boynard^{8,9}, Martyn P. Chipperfield^{1,2}, Wuhu Feng^{1,10}, Matilda A. Pimlott¹, Sandip S. Dhomse^{1,2}, Christian Retscher¹¹, Catherine Wespes¹² and Richard Rigby^{1,13}

13: Centre for Environmental Modelling and Computation, University of Leeds, Leeds, United Kingdom

Ozone is a potent air pollutant in the lower troposphere and an important short-lived climate forcer (SLCF) in the upper troposphere. Studies investigating long-term trends in tropospheric column ozone (TCO_3) have shown large-scale spatiotemporal inconsistencies. Here, we investigate the long-term trends in lower tropospheric column ozone (LTCO_3 , surface-450 hPa sub-column) by exploiting a synergy of satellite and ozonesonde datasets and an Earth System Model (UKESM) over North America, Europe and East Asia for the decade 2008-2017. Overall, we typically find small LTCO_3 linear trends with large uncertainty ranges from the Ozone Monitoring Instrument (OMI) and the Infrared Atmospheric Sounding Interferometer (IASI), while model simulations indicate a stable LTCO_3 tendency. Trends in the satellite a priori datasets show negligible



trends indicating year-to-year sampling is not an issue. The application of the satellite averaging kernels (AKs) to the UKESM ozone profiles, accounting for the satellite vertical sensitivity and allowing for like-for-like comparisons, has a limited impact on the modelled LTCO₃ tendency in most cases. While, in relative terms, this is more substantial (e.g. in the order of 100%), the absolute magnitudes of the model trends show negligible change. However, as the model has a near-zero tendency, artificial trends were imposed on the model time-series (i.e. LTCO₃ values rearranged from smallest to largest) to test the influence of the AKs but simulated LTCO₃ trends remained small. Therefore, the LTCO₃ tendency between 2008 and 2017 in northern hemispheric regions are likely small, with large uncertainties, and it is difficult to detect any small underlying linear trends due to inter-annual variability or other factors which require further investigation.

1. Introduction

Tropospheric ozone (TO₃) is a short-lived climate forcer (SLCF) and an important greenhouse gas (GHG; Myhre et al., 2013; Forster et al., 2021). TO₃ is also a hazardous air pollutant with adverse impacts on human health (Doherty et al., 2017; WHO, 2022) and agricultural/natural vegetation (Sitch et al., 2007; Hollaway et al., 2012). Since the pre-industrial (PI) period, anthropogenic activities have increased the atmospheric loading of ozone (O₃) precursor gases, most notably methane (CH₄) and nitrogen oxides (NO_x) resulting in an increase in TO₃ of 25-50% since 1900 (Gauss et al., 2006; Lamarque et al., 2010; Young et al., 2013). The PI to present day (PD) radiative forcing (RF) from TO₃ is estimated by the Intergovernmental Panel on Climate Change (IPCC) to be 0.47 Wm⁻² (Forster et al., 2021) with an uncertainty range of 0.24-0.70 Wm⁻².

During the satellite-era (i.e. since the mid-1990s), extensive records of TO₃ have been produced, e.g. by the European Space Agency Climate Change Initiative (ESA-CCI; ESA, 2019). However, the large presents of stratospheric O₃, coupled with the different vertical sensitivities and sources of error associated with observations in different wavelength regions (e.g. Eskes and Boersma 2003; Ziemke et al., 2011; Miles et al., 2015) means large-scale inconsistencies in time and space exist between the records of satellite tropospheric column ozone (TCO₃) (as shown by Gaudel et al., 2018).

The work by Gaudel et al. (2018) was part of the Tropospheric Ozone Assessment Report (TOAR), which represented a large global effort to understand spatio-temporal patterns and variability in TO₃. However, their investigation of ozonesondes (2003-2012) and products from nadir viewing satellites in polar orbits (three from the Ozone Monitoring Instrument (OMI) (2005-2015/6) and two from the Infrared Atmospheric Sounding Interferometer (IASI) (2008-2016)) displayed discrepancies in the spatial distribution, magnitude, direction and significance of the TCO₃ trends. They noted that the records cover slightly different time periods but were unable to provide any definitive reasons for these discrepancies beyond briefly suggesting that differences in measurement techniques and retrieval methods were likely to be causing the observed spatial inconsistencies.

The vertical sensitivity of each retrieved product (function of measurement technique and retrieval methodology) used by Gaudel et al. (2018) will have had an impact on which part of the troposphere the O₃ signal is weighted towards. This was evident in the OMI and IASI TCO₃ trends, where OMI showed predominantly positive trends between 60°S and 60°N while the opposite was the case for IASI. The vertical sensitivity is represented by the “averaging kernel” (AK), which provides the relationship between perturbations at different levels in the retrieved and true profiles (Eskes and Boersma, 2003). Typically, for the products used by Gaudel et al., (2018), the peak AK sensitivities for TO₃ are in the 0-6 km range for OMI (Miles et al., 2015) and around 11-12 km for IASI (Keim et al., 2009). In the case of the Rutherford Appleton Laboratory (RAL) Space OMI data, used in Gaudel et al., (2018), TCO₃ values were derived from retrieved surface – 450hPa layer average mixing ratios applied also to the overlying 450hpa – tropopause layer using



ERA-Interim profiles. As the TO_3 values were derived from different (UV and IR) sensors and methodologies whose vertical sensitivities differ, they were likely representing O_3 controlled by different contributions of atmospheric processes (e.g. precursor emissions from the surface and stratosphere-troposphere exchanges). Therefore, TCO_3 trends from the different satellite products are not necessarily expected to be similar.

In this study, we undertake the first assessment of spatio-temporal variability in satellite-derived lower tropospheric column ozone (LTCO_3 , surface-450 hPa) from three instruments over a consistent decade (2008-2017). In combination with an Earth System Model (ESM), we aim to quantify the impact of year-to-year sampling, the satellite instrument uncertainties and the instrument vertical sensitivity on long-term LTCO_3 trends. We focus our analysis on North America, Europe and East Asia given their large emissions of ozone precursor gases and temporal variability. In our manuscript, **Section 2** discusses the satellite/ozonesonde datasets and model used, **Section 3** presents our results, and our discussion/conclusions are summarised in **Sections 4 and 5**.

2. Methodology and Datasets

2.1. Satellite Datasets

The satellite products (see **Table 1**) used here are from nadir-viewing polar-orbiting platforms providing ozone sub-column profiles. This includes ozone profile data from the OMI product developed by the RAL Space and the IASI products from the Laboratoire d'aérodynamique (IASI-SOFRID) and the Université Libre de Bruxelles, in collaboration with the Laboratoire Atmosphères, Observations Spatiales (ULB-LATMOS) (IASI-FORLI). OMI and IASI are on NASA's Aura and Eumetsat's MetOp-A satellites in sun-synchronous low Earth orbits with local overpass times of 13.30 and 9.30, respectively. OMI and IASI are ultraviolet-visible (UV-Vis) and infrared (IR) sounders with spectral ranges of 270-500 nm (Boersma et al., 2008, Boersma et al., 2011) and $645\text{--}2760\text{ cm}^{-1}$ (Illingworth et al., 2011), respectively. OMI has a spatial footprint at nadir of $24\text{ km} \times 13\text{ km}$, while IASI measures simultaneously in four fields of view (FOV, each circular at nadir with a diameter of 12 km) in a $50\text{ km} \times 50\text{ km}$ square which are scanned across track to sample a 2200 km-wide swath (Clerbaux et al., 2009). The OMI retrieval scheme is based on an optimal estimation (OE) approach, produced by RAL Space, which is described in detail by Miles et al., (2015). The retrieval schemes for IASI-FORLI and IASI-SOFRID O_3 are discussed in detail by Boynard et al., (2018) and Barret et al., (2020). In this work, the OMI data were filtered for good quality retrievals where the geometric cloud fraction was <0.2 , the sub-column O_3 values were >0.0 , the solar zenith angle $<80.0^\circ$, the retrieval convergence flag = 1.0 and the normalised cost function was <2.0 . The IASI-FORLI data were filtered for a geometric cloud fraction <0.13 (pre-filtered), degrees of freedom >2.0 , O_3 values >0.0 , solar zenith angle $<80.0^\circ$ and the surface to 450 hPa sub-column O_3 / total column $\text{O}_3 < 0.085$. The IASI-SOFRID data were provided on a $1.0^\circ \times 1.0^\circ$ horizontal grid (i.e. level 3 product, but at a daily temporal resolution – we use the daytime data in this study) with filtering already applied in Barret et al., (2020). Here, only O_3 values >0.0 were used. To remove systematic biases between the satellite records, ozonesondes were used to generate bias correction factors (2008-2017) to help harmonise the data sets. This is discussed in the Supplementary Material (i.e. **S1**). The application of the satellite AKs to the ozonesondes and the model is also discussed in **S1**. To investigate long-term trends over North America, Europe and East Asia, the Hemispheric Transport of Air Pollution (HTAP) regional sea-land mask (European Commission (2016); see **S2, Figure S2**), is used to generate average monthly time-series for each product over each region of interest. In Section 3.2, where we discuss the impact of satellite retrieval errors on derived LTCO_3 linear trends, the OMI and IASI-FORLI retrieval errors are provided in their product files, but are not available for IASI-SOFRID. Therefore, while not a perfect metric to represent the error in the IASI-SOFRID data, we use the standard deviation in the monthly-spatial average of the regional time-series.



125 2.2. United Kingdom Earth System Model (UKESM)

126 The UK's Earth System Model, UKESM1.0, is a state-of-the-art ESM with fully interactive coupled component
127 models (e.g. atmosphere, ocean, land surface, atmospheric chemistry), which has been developed by the UK
128 Met Office and the Natural Environment Research Council (NERC). The detailed coupling of all the Earth
129 System components is described by Sellar et al. (2019). However, in this study, we run UKESM1.0 in an
130 atmosphere only configuration (e.g. similar to Archibald et al., (2020)). The aim is to use UKESM1.0 to
131 investigate long-term trends in TO₃ and help explore inconsistencies between satellite records, so it is
132 computationally more time efficient as only the atmospheric dynamics and chemistry components are
133 simulated. Over the 2008-2017 time period (with a 1-year spin up), the UKESM1.0 model tracers and
134 diagnostics (e.g. ozone, pressure) are output as 3D fields at sub-daily (6-hourly) time steps to allow robust
135 comparisons between the model and satellite data sets (i.e. model-satellite spatio-temporal co-location to
136 reduce representation biases and application of the satellite AKs to map the instrument vertical sensitivity
137 onto the model yielding like-for-like comparisons).

138 Here, the UKESM1.0 land and atmosphere share a regular latitude–longitude grid with a resolution of 1.25°
139 ×1.875° with 85 vertical levels on a terrain-following hybrid height coordinate with a model lid at 85 km
140 above sea level (50 levels are below 18 km). All the key inputs to the model from other Earth system
141 components (e.g. sea surface temperature (SST) and land surface vegetation) were prescribed from ancillary
142 files. The ocean and ice forcing are represented by the monthly Reynolds sea ice and SSTs data from the
143 National Oceanic and Atmospheric Administration (NOAA, [https://climatedataguide.ucar.edu/climate-](https://climatedataguide.ucar.edu/climate-data/)
144 [data/](https://climatedataguide.ucar.edu/climate-data/)). Solar forcings are provided by Phase 6 of the Coupled Model Intercomparison Project (CMIP6;
145 Matthes et al., 2017; Eyring et al., 2016), as is the stratospheric aerosol climatology to represent
146 contributions from volcanic eruptions (Sellar et al., 2019). The land cover is provided from output from the
147 land surface component of the ESM (JULES; Wiltshire et al., 2021) from a fully coupled historical simulation.
148 Anthropogenic and biomass burning emissions from Hoesly et al. (2018) and van Marle et al. (2017) are
149 prescribed for the period 2008 to 2014. After 2014, anthropogenic and biomass burning emissions are from
150 the Shared Socioeconomic Pathway (SSP, Rao et al., 2017) 2-4.5 (i.e. a middle-of-the-road climate and
151 emissions scenario).

152 Biological emissions are a climatology between 2001 and 2010 from the MEGAN-MACC data base
153 (Sindelarova et al., 2014), while natural emissions are from the Precursors of Ozone and their Effects in the
154 Troposphere (POET, http://accent.aero.jussieu.fr/database_table_inventories.php) based on 1990. Dry
155 deposition of O₃ to the land surface is represented by the Wesley scheme, which is applied as in O'Connor et
156 al., (2014). The model is also in a nudged or “specified dynamics” configuration (i.e. meteorological analyses
157 are used to “nudge” the model's meteorological variables, i.e. u- and v-wind components, and potential
158 temperature, towards reality; Telford et al., 2008) using 6-hourly reanalysis data from the European Centre
159 for Medium-Range Weather Forecasts (ECMWF) ERA-Interim product. A similar configuration of UKESM1.0
160 was used by Archibald et al., (2020), in which a thorough evaluation against multiple observations (e.g.
161 surface, aircraft and satellite) was carried out.

162 2.3. Trend Approach

163 LTCO₃ trends are calculated using the linear least squares fit approach of van der A et al., (2006; 2008), and
164 utilised by Pope et al., (2018) who investigated LTCO₃ trends. Here, the monthly LTCO₃ time-series are
165 represented by the function:

$$166 \quad Y_t = C + BX_t + A\sin(\omega X_t + \phi) + N_t \quad (1)$$



167 where Y_t is the observed monthly LTCO_3 for month t , X_t is the number of months since the start of the record,
168 C is the first month of the record, B is the monthly linear trend and $\text{Asin}(\omega X_t + \phi)$ is the seasonal model
169 component (Weatherhead et al., 1998). A is the amplitude, ω is the frequency (set to 1 year; $\omega = \pi/6$) and ϕ is
170 the phase shift. C , B , A and ϕ are the fit parameters from the linear least squares fit. N_t represents the model
171 errors/residuals. The linear trend uncertainty, σ_B , represents the trend precision and is calculated as:

172
$$\sigma_B = \left[\frac{\sigma_N}{n^2} \sqrt{\frac{(1+\alpha)}{(1-\alpha)}} \right] \quad (2)$$

173 where n is the number of years, α is the autocorrelation in the residuals (N_t) and σ_N is the standard deviation
174 in the residuals. As in van der A et al., (2006) and Pope et al., (2018), we calculate the autocorrelation for each
175 time-series using a lag of one-time step (i.e. one month). The autocorrelation in **Equation 1** is not accounted
176 for directly, so is factored into the trend uncertainty (**Equation 2**), as used and discussed by van der A et al.,
177 (2006) and Weatherhead et al., (1998), respectively.

178 **3. Results**

179 A detailed evaluation of UKESM1.0 LTCO_3 through comparisons with the three satellite products and
180 ozonesondes is presented in **S3**. Overall, UKESM1.0 robustly simulates LTCO_3 spatially and seasonally in
181 comparison to the ozonesondes and satellite instruments (i.e. typically within the ozonesonde variability and
182 satellite uncertainty range).

183 **3.1. UKESM1.0 and Satellite LTCO_3 Trends**

184 LTCO_3 trends from OMI, IASI-FORLI, IASI-SOFRID and ozonesondes are derived between 2008 and 2017 (i.e.
185 consistent time record for all instruments) using the linear-seasonal trend model (**Equation 1**). For each
186 satellite product, the corresponding UKESM1.0 time-series (with and without AKs) are analysed as well as
187 the satellite apriori. For the North America OMI metrics (**Figure 1 – top left, Table 2**), there is clear
188 seasonality in the apriori ranging between approximately 17.0 and 22.0 Dobson Units (DU). As this is based
189 on the climatology of McPeters et al., (2007), there is no trend and there is a very good model fit (i.e.
190 $R^2=1.0$). The key point is that, as a climatology, the apriori will have no trend but if there are substantial
191 temporal sampling differences between years, then an artificial trend could be introduced. OMI LTCO_3
192 ranges between 20.0 and 27.0 DU with substantial variability. There is a drop in LTCO_3 to 19.0 DU in 2009
193 before peaking at 25.0-27.0 DU between 2010 and 2015. Peak LTCO_3 then drops to 22.0-24.0 DU in 2016 and
194 2017. As a result, the linear-seasonal trend model, which does not account for interannual variations such as
195 this, only has a fit skill of $R^2=0.59$. The corresponding OMI LTCO_3 trend is -0.79 (-7.07, 5.48; 95% confidence
196 interval, p-value = 0.80) DU/decade showing a negligible trend with a large uncertainty range. Here, -0.79
197 DU/decade is the trend while the -7.07 and 5.48 DU/decade values are the 95% confidence interval. The
198 UKESM1.0 LTCO_3 time-series ranges between 17.0 and 22.0 DU with clear seasonality, though somewhat less
199 inter-annual variation than OMI, and the linear-seasonal trend model therefore has a considerably better fit
200 with $R^2=0.95$. The model trend has the opposite sign at 0.21 (-0.37, 0.78; p = 0.59) DU/decade. Here, the
201 model trend is near-zero with a relatively large uncertainty range (though not as sizable as OMI). When the
202 AKs are applied to the model, the trend switches sign to -0.57 (-1.58, 0.45, p = 0.98) DU/decade and the
203 linear-seasonal trend model fit decreases in skill to $R^2=0.90$. The trend switch of sign, though small, is
204 potentially linked to the application of the AKs, which also increases LTCO_3 by 2.0-3.0 DU in general.

205 The IASI-FORLI LTCO_3 time-series (**Figure 1 – top right**) tends to be lower than OMI and range between 17.0
206 and 22.0 DU. There is a substantial negative IASI-FORLI trend (-1.42 (-2.35, -0.50; p = 0.00) DU/decade);
207 **Table 2**) though as suggested by Boynard et al., (2018) and Wespes et al., (2018), the input IASI Level-1 data



sets into the FORLI retrieval are not consistent with time; they suffer from a specific discontinuity in September 2010 which degrades the robustness of this trend. While we are aware of the artificial trend in the IASI-FORLI dataset, it is still a valuable long-term product allowing us to quantify multiple factors (e.g. impact of AKs on model tendencies/absolute values and year-to-year sampling stability – i.e. near-zero trend in the apriori). The apriori has a negligible trend but there is no clear seasonality in the apriori time-series. As a result, the linear-seasonal trend model has a more limited fit skill (i.e. $R^2=0.67$). The impact of the satellite AKs appears to have less impact for IASI-FORLI as both UKESM1.0 and UKESM1.0+AKs have time-series ranging between approximately 17.0 and 21.0 (though slightly smaller UKESM1.0+AKs range) and linear-seasonal trend model fits of $R^2=0.93$ and $R^2=0.92$, respectively. The corresponding trends are small at -0.13 (-0.75, 0.49; $p = 0.67$) and -0.32 (-0.82, 0.20; $p = 0.22$) DU/decade, but the introduction of the AKs does move the UKESM1.0 trend slightly towards that of the satellite. For IASI-SOFRID (**Figure 1 – bottom left**), there is little difference between any of the time-series as they all range between 16.0 and 21.0 DU with corresponding linear-seasonal trend model fits of $R^2=0.94$ to 0.98 and negligible trends. The IASI-SOFRID and apriori trends are 0.12 (-0.59, 0.82; $p = 0.74$) and 0.11 (-0.17, 0.39; $p = 0.43$) DU/decade; **Table 2**), respectively, with the model showing near-zero trends in both cases. Given the close agreement between the satellite and apriori time series and fit metrics, it is suggestive that IASI-SOFRID TO_3 is more closely confined to the apriori profile than are the other products. The ozonesondes show a substantial trend of -1.15 (-2.0, -0.10; $p = 0.03$) DU/decade, while the model trend sampled as the sondes is -0.16 (-1.67, 1.35; $p = 0.63$) DU/decade. The co-located model and ozonesonde linear-seasonal trend model fits are $R^2=0.62$ and 0.64, respectively. The noise and lack of seasonality in the ozonesonde time-series is slightly unexpected given the reasonable density of stations over North America, though the spatial coverage and temporal sampling is much less than the satellite products.

In Europe, the OMI LTCO_3 values are larger than in North America, ranging between 19.0 and 30.0 DU (**Figure 2 – top left**). The same inter-annual variability exists, peaking between 2010 and 2015 with the minimum in 2009. Hence, the linear-seasonal trend model, which does not represent interannual variation, does not have high skill and $R^2=0.72$. The corresponding trend is -0.80 (-7.29, 5.69; $p = 0.80$) DU/decade, so has a similar direction and magnitude to that for North America, though is not substantial. The apriori ranges between 17.0 and 22.5 DU with a trend of -0.12 (-0.26, 0.03; $p = 0.10$; **Table 2**) DU/decade. Given the relatively small trend and uncertainty range, unlike the OMI equivalent, it suggests there is unlikely to be an artificial trend arising through year-to-year changes in geographical sampling across the European region. UKESM1.0 LTCO_3 ranges between approximately 19.0 and 22.0 DU with a good linear-seasonal trend model fit of $R^2=0.99$ and a trend of -0.11 (-0.50, 0.29; $p = 0.59$) DU/decade. As for North America, when the OMI AKs are applied, the UKESM LTCO_3 values systematically increase by 2.0-3.0 DU, move further away from the satellite apriori and more closely follow the variability of OMI (although R^2 decreases slightly to 0.95). The trend tends towards that of OMI at -0.72 (-1.77, 0.32; $p = 0.16$) DU/decade. As in the case of North America, the European IASI-FORLI apriori has no seasonal cycle (and moderate R^2 of 0.48 in the linear-seasonal trend model fit) with a near-zero trend (0.09 (-0.09, 0.27; $p = 0.32$) DU/decade) (**Figure 2 – top right, Table 2**). The IASI-FORLI data exhibit a substantial negative trend of -1.83 (-2.78, 0.89; $p = 0.00$) DU/decade, again potentially attributable to step changes in the IASI Level-1 processor, with a good linear-seasonal trend model fit of $R^2=0.92$. UKESM1.0 LTCO_3 trends, without and with AKs applied, are -0.28 (-0.77, 0.20; $p = 0.25$) and -0.43 (-1.21, 0.35; $p = 0.27$) DU/decade. Again, though a small change, the application of the AKs introduces a slight perturbation of the model trend compared to IASI-FORLI. The IASI-SOFRID apriori, ranging between 17.0 and 21.0 DU, has a trend of 0.17 (-0.12, 0.45; $p = 0.24$) DU/decade with good fit skill of $R^2=0.98$ (**Figure 2 – bottom left**). The IASI-SOFRID and UKESM1.0 metrics, with and without averaging kernels



applied, are similar, with LTCO_3 trends of 0.05 (-0.91, 1.01; $p = 0.92$), -0.27 (-0.72, 0.19; $p = 0.24$) and 0.08 (-0.33, 0.49; $p = 0.69$) DU/decade, respectively, and with R^2 values between 0.93 and 0.98. The ozonesonde monthly regional means (**Figure 2 – bottom right**) has a more pronounced time-series than North America, yielding a less noisy time-series of LTCO_3 . Here, there is clear seasonality ranging between 17.0 and 24.0 DU with a large R^2 value of 0.95. The ozonesonde trend is relatively small at -0.61 (-1.39, 0.17; $p = 0.12$) DU/decade while the UKESM1.0 equivalent is more substantial at -0.96 (-1.56, 0.35; $p = 0.00$) DU/decade.

For East Asia, OMI LTCO_3 again has both a pronounced seasonal cycle and inter-annual variability (19.0-27.0 DU), consistent with the other two regions discussed above (**Figure 3 – top left**). This yields a moderate skill fit to the linear-seasonal trend model of $R^2=0.52$ and near-zero trend (-0.09 (-7.88, 7.70; $p = 0.98$) DU/decade). The apriori has a trend of -0.25 (-0.71, 0.22; $p = 0.29$) DU/decade, so year-to-year sampling changes could be influencing the robustness of OMI retrieved time-series in this region. However, both the instrument and apriori trend uncertainties intersect with 0.0. UKESM1.0 LTCO_3 ranges between approximately 16.0 and 22.0 DU with a good fit R^2 of 0.98. Like the other regions, the application of the OMI AKs increases the model values systematically by several DUs. The UKESM1.0 LTCO_3 trend is -0.16 (-0.94, 0.62; $p = 0.67$) DU/decade, which is small, but the AKs increase the trend magnitude to -0.62 (-2.24, 1.00; $p = 0.44$) DU/decade, which moves it away from the OMI trend. IASI-FORLI (**Figure 3 – top right, Table 2**), like the other two regions, has a substantial negative trend of -1.52 (-2.16, 0.88; $p = 0.00$) DU/decade. The apriori again exhibits virtually no seasonal cycle but non-zero year-to-year variation so a low fit skill of $R^2=0.21$ and shows a near-zero trend of -0.03 (-0.22, 0.16; $p = 0.76$) DU/decade. For UKESM1.0, the East Asian seasonal range is much larger than other regions, ranging between 17.0 and 27.0 DU (i.e. seasonal amplitude of approximately ± 5.0 DU). When the AKs are applied, this range shrinks to approximately 19.0 to 23.0 DU, more in-line with the IASI-FORLI LTCO_3 values. The corresponding model trends are -0.03 (-0.62, 0.56; $p = 0.93$) DU/decade and -0.29 (-0.80, 0.22; $p = 0.25$) DU/decade, so the AKs are pushing the model tendency towards that of the instrument, though the impact is small in absolute terms (large in relative terms). IASI-SOFRID and its apriori LTCO_3 seasonality are again very similar, ranging between 16.0 and 21.0 DU with very little interannual variability and with linear seasonal trend model fit skills of $R^2=0.96$ and 0.98 (**Figure 3 – bottom left, Table 2**). The IASI-SOFRID and apriori linear trends are therefore also consistent at -0.19 (-1.01, 0.63; $p = 0.65$) and -0.15 (-0.73, 0.58; $p = 0.82$) DU/decade. The UKESM1.0 seasonal variability is again large, between 17.0 and 26.0 DU, and, as in the case of IASI-FORLI, when the instrument AKs are applied to the model, the seasonal range shrinks (i.e. 16.0-22.0 DU) to be much closer to those of the retrieval and its prior. The model trends are -0.42 (-0.97, 0.13; $p = 0.12$) and -0.24 (-0.67, 0.20; $p = 0.28$) (with AKs) DU/decade, where there is a minor shift in the model tendency towards that of IASI-SOFRID and its prior. For the ozonesondes (**Figure 3 – bottom right**), there is a substantial LTCO_3 trend of 3.17 (0.16, 6.17; $p = 0.04$) DU/decade with a fit skill of $R^2=0.79$, which is larger than those for North America and Europe. LTCO_3 increases from 18.0-25.0 in 2008 to 21.0-28.0 in 2011. This remains similar in 2012 and 2013 before dropping by several DUs between 2014 and 2017. The UKESM1.0 sampled as the ozonesondes has considerably less inter-annual variability with a smaller trend of 0.37 (-0.90, 1.64; $p = 0.56$) DU/decade. Therefore, UKESM1.0 and the satellite product trends are generally smaller (in magnitude) than the ozonesonde tendencies. However, it is worth considering that there are only a few sites (e.g. Hong Kong and Taiwan) where ozonesonde data is available in East Asia.

3.2. Influence of Satellite Averaging Kernels on UKESM1.0 LTCO_3

To investigate the impact of applying the satellite averaging kernels to UKESM1.0, and thus learn something about vertical sensitivity influence on retrieved LTCO_3 , three different metrics are considered for the 2008 to 2017 time-period. These are the absolute LTCO_3 value, amplitude of the LTCO_3 seasonal cycle and the linear



296 trend. These metrics are compared for the satellite, the satellite \pm error term, the apriori, UKESM1.0 and
297 UKESM1.0+AKs for the three regions discussed above.

298 From **Figure 4**, average OMI L_{TCO₃} is approximately 22.0, 24.0 and 23.0 DU for North America, Europe and
299 East Asia, respectively. This represents a substantial deviation away from the apriori values of 17.5, 20.0 and
300 16.0 DU, respectively. However, the average error term for OMI L_{TCO₃} is sizeable at approximately ± 8.0 to
301 ± 9.0 DU for all regions. The average UKESM1.0 value for each region is approximately 19.5, 21.5 and 19.0 DU
302 but the application of the AKs increases this by several DU to 22.0, 24.0 and 21.0 DU. In comparison, mean
303 values for both IASI products vary less between the three geographical areas: IASI-FORLI (IASI-SOFRID) L_{TCO₃}
304 values are 20.0 (18.5), 19.0 (18.5) and 22.0 (18.0) DU, respectively. The corresponding error ranges, in
305 comparison with OMI, are smaller between 17.0 and 23.0 (16.0 and 21.5), 16.0 and 21.5 (16.0 and 21.0) and
306 18.0 and 23.5 (14.5 and 21.5) DU for North America, Europe and East Asia, respectively. With the IASI-FORLI
307 AKs applied to UKESM1.0, L_{TCO₃} decreases from 19.5 to 19.25 DU, 21.25 to 19.5 DU and 22.75 to 21.25 DU
308 for the three regions. For IASI-SOFRID, there is a decrease from 21.0 to 19.5 DU in Europe and a decrease
309 from 22.0 to 19.5 DU in East Asia, while no change occurs in North America. Overall, OMI has the largest
310 error range and the application of the AKs to UKESM1.0 systematically increases the model L_{TCO₃} time-
311 series by several DU. The opposite occurs for the IASI products where there is a smaller decrease to
312 UKESM1.0 L_{TCO₃} of 1.0-2.0 DU. The error ranges are also smaller than that of OMI.

313 In terms of the L_{TCO₃} seasonal amplitude (**Figure 5**), OMI (including the error terms) is approximately 2.6
314 (for all) DU, 3.3-3.8 DU and 2.3-2.6 DU for North America, Europe and East Asia. The apriori seasonal
315 amplitude ranges from 2.7 to 2.9 DU across the regions. The IASI-FORLI averages (including the error terms)
316 tend to be lower than OMI but have similar seasonal ranges. North America, Europe and East Asia have
317 amplitudes of 2.3-2.5 DU, 2.3-2.5 DU and 1.6-1.8 DU, respectively. It is noteworthy that this seasonal cycle is
318 despite the IASI-FORLI prior exhibiting virtually no seasonal cycle at all. IASI-SOFRID has a European range of
319 2.4-2.6 DU, and comparable ranges for North America and East Asia at 1.8-2.5 DU and 2.3-3.0 DU. Therefore,
320 seasonal amplitude in IASI-SOFRID is more sensitive to the error metric but as the “error” term is based on
321 the L_{TCO₃} standard deviation, given the lack of an error term in the product, it is unsurprising that there is
322 more variability in the seasonal amplitude. For the OMI comparisons, the application of the AKs to
323 UKESM1.0 shifts the simulated amplitude slightly upwards from 2.0 to 2.1 DU, 3.1 to 3.3 DU and 4.0 to 4.4
324 DU for the respective regions. The IASI-FORLI AK impacts are a decrease from 1.9 to 1.4 DU, 3.0 to 2.1 DU
325 and 4.2 to 1.9. For IASI-SOFRID, the corresponding impact on UKESM1.0 is 2.2 to 2.4 DU, 3.3 to 2.9 and 4.5 to
326 3.2 DU. Therefore, the OMI AKs have a minimal impact, increasing the model seasonal amplitude by 0.1-0.3
327 DU, but the IASI products suppress the simulated amplitude by 1.0-2.0 DU at the most extreme.

328 The impact of the satellite L_{TCO₃} error terms on the derived linear trends are shown in **Figure 6**. For OMI,
329 the range in trends calculated (i.e. satellite \pm error term) is approximately -1.50 (-7.04, 4.04; $p = 0.59$) to -
330 0.09 (-6.98, 6.81; $p = 0.98$) DU/decade, -1.65 (-6.92, 3.62; $p = 0.53$) to 0.05 (-7.44, 7.53; $p = 0.99$) DU/decade
331 and -1.05 (-6.61, 4.52; $p = 0.70$) to 0.87 (-8.24, 9.98; $p = 0.85$) DU/decade for North America, Europe and East
332 Asian, respectively. The IASI-FORLI trends (i.e. satellite \pm error term) are substantial, ranging from -1.50 (-
333 2.51, -0.50; $p = 0.00$) to -1.34 (-2.21, -0.47; $p = 0.00$) DU/decade, -1.87 (-2.87, -0.87; $p = 0.00$) to -1.80 (-2.72, -
334 0.88; $p = 0.00$) DU/decade and -1.62 (-2.27, -0.98; $p = 0.00$) to -1.42 (-2.06, -0.78; $p = 0.00$) for the three
335 regions, respectively. The corresponding IASI-SOFRID trends were 0.09 (-0.48, 0.66; $p = 0.75$) to 0.14 (-0.59,
336 0.88; $p = 0.70$) DU/decade, -0.07 (-0.91, 0.78; $p = 0.87$) to 0.16 (-0.74, 1.07; $p = 0.72$) DU/decade and -0.30 (-
337 1.02, 0.42; $p = 0.41$) to -0.08 (-0.73, 0.58; $p = 0.82$), respectively. Therefore, only the IASI-FORLI trends (i.e.
338 satellite \pm error term) are substantially different from zero (i.e. $p < 0.05$). However, that is likely due in part



339 to discontinuities in the Level-2 input meteorological data used to generate this version of the product
340 (Boynard et al., 2018).

341 The application of the OMI AKs to UKESM1.0 had the largest impacts on the simulated trends with changes
342 in a negative direction from of 0.21 (-0.37, 0.78; $p = 0.59$) to -0.57 (-1.58, 0.45, $p = 0.98$) DU/decade, -0.11 (-
343 0.50, 0.29; $p = 0.59$) to -0.72 (-1.77, 0.32; $p = 0.16$) DU/decade and -0.16 (-0.94, 0.62; $p = 0.67$) to -0.62 (-
344 2.24, 1.00; $p = 0.44$) DU/decade for the respective regions. IASI-FORLI AKs introduced small decreases from -
345 0.13 (-0.75, 0.49; $p = 0.67$) to -0.32 (-0.82, 0.20; $p = 0.22$) DU/decade, -0.28 (-0.77, 0.20; $p = 0.25$) to -0.43 (-
346 1.21, 0.35; $p = 0.27$) DU/decade and -0.03 (-0.62, 0.56; $p = 0.93$) to -0.29 (-0.80, 0.22; $p = 0.25$) DU/decade.
347 IASI-SOFRID AKs introduced small increases in the LTCO₃ trend from -0.24 (-0.85, 0.37; $p = 0.44$) to -0.04 (-
348 0.53, 0.45; $p = 0.87$) DU/decade, -0.27 (-0.72, 0.19; $p = 0.24$) to 0.08 (-0.33, 0.49; $p = 0.69$) DU/decade and -
349 0.42 (-0.97, 0.13; $p = 0.12$) to -0.24 (-0.67, 0.20; $p = 0.28$) DU/decade.

350 As the absolute model trends are small, it is difficult to determine the impact of the AKs on the simulated
351 trends. In relative terms, it can have impacts of several 100% but the model and model+AK trend ranges
352 (95% confidence interval) always intersect. Therefore, in an attempt to derive more substantial UKESM1.0
353 LTCO₃ trends (without and with AKs applied), to assess the maximum impact the AKs can have on UKESM
354 LTCO₃ trends, the modelled data were sorted from lowest to highest and the trend re-calculated. In North
355 America, this approach forced positive model trends, sub-sampled to OMI, IASI-FORLI and IASI-SOFRID, of
356 0.73 (0.22, 1.25; $p = 0.00$), 0.64 (-3.50, 4.77; $p = 0.76$) and 0.80 (0.41, 1.19; $p = 0.00$) DU/decade. When the
357 AKs were applied, it yielded trends of -0.74 (-1.89, 0.40; $p = 0.20$), 0.55 (0.08, 1.03; $p = 0.02$) and 0.58 (0.24,
358 0.92; $p = 0.00$) DU/decade. In Europe, this forced positive trends model trends, of 0.62 (0.14, 1.10; $p = 0.01$),
359 0.37 (-0.05, 0.79; $p = 0.08$) and 0.46 (0.09, 0.84; $p = 0.01$) DU/decade, respectively. With the AKs applied, the
360 trends become 0.47 (-0.51, 1.44; $p = 0.34$), 0.28 (-0.38, 0.94; $p = 0.40$) and 0.10 (-0.32, 0.51; $p = 0.64$)
361 DU/decade. Finally, in East Asia, the forced model trends are 0.90 (0.34, 1.47; $p = 0.00$), 0.66 (0.15, 1.17; $p =$
362 0.01) and 0.63 (0.26, 1.00; $p = 0.00$) DU/decade. The application of the AKs introduced model trends of 1.02
363 (-0.04, 2.09; $p = 0.05$), 0.08 (-0.44, 0.61; $p = 0.75$) and 0.20 (-0.20, 0.61; $p = 0.31$) DU/decade.

364 Even with forced trends in the UKESM1.0 regional time-series, the trends are relatively small (i.e. typically
365 less than 1.0 DU/decade in magnitude). Therefore, the application of the AKs to the forced UKESM LTCO₃
366 time-series still yields small scale change tendencies and there is overlap in the two model trend uncertainty
367 ranges (i.e. 95% confidence level). However, in relative terms, the trend changes are larger (e.g. >100% in
368 multiple cases) and there is often a shift of the modelled LTCO₃ trend uncertainty range either intersecting
369 or no longer intersecting with zero (i.e. a shift in p -value regime from <0.05 to >0.05). Therefore, in modelled
370 and satellite datasets with more substantial trends, the impacts of the AKs, and thus the satellite vertical
371 sensitivity, on LTCO₃ trends would be much greater and potentially help pinpoint sources of differences
372 between satellite products in their TO₃ temporal evolution.

373 4. Discussion

374 Investigation of satellite LTCO₃ focussed on 2008 to 2017, representing a decade of overlap of the OMI and
375 IASI records. The analysis focussed on North America, Europe and East Asia as these regions are subject to
376 large emissions of and temporal changes in O₃ precursor gases. LTCO₃ is typically spatially homogeneous
377 with shallow gradients between background and source-induced O₃ concentrations. Secondly, individual
378 retrievals of LTCO₃ are subject to multiple issues (e.g. influences on radiative transfer and vertical sensitivity
379 of stratospheric ozone, cloud and other particulates, surface spectral reflectivity/emissivity and temperature
380 profile) which can result in noisy LTCO₃ time-series at high resolution (e.g. when gridded on a scale of 0.5° or
381 1.0°). Both of these factors supported analysis at a regional scale (e.g. continental scale).



382 Ideally, this analysis would have utilised several more records (e.g. several UV-Vis and IR products) to
383 quantify long-term trends in LTCO_3 and investigate the potential reasons for any discrepancies, as shown by
384 Gaudel et al., (2018) for TCO_3 . While RAL Space, and other providers, have generated UV-Vis profile O_3
385 products for more instruments, e.g. from the Global Ozone Monitoring Experiment 1 & 2 (GOME-1 & GOME-
386 2) and the SCanning Imaging Absorption spectroMeter for Atmospheric CartographY (SCIAMACHY), the
387 GOME-1 and SCIAMACHY records do not overlap for as long with IASI and step changes in the GOME-2A
388 Level-1 processing scheme used to produce the available LTCO_3 Level-2 version mean it is not sufficiently
389 homogeneous (see Pope et al., (2023)). For the IR instruments, other potential sensors include the
390 Tropospheric Emissions Spectrometer (TES; Richards et al., 2008) and the RAL Space IASI Extended Infrared
391 Microwave Sounding (IMS; Pimlott et al., 2022) scheme applied to IASI. Unfortunately, the TES record only
392 covers 2005 to 2013, with decreasing spatial coverage with time, and at the time of this work the IASI-IMS
393 product had only been processed on a sub-sampled basis of 1 in 10 days.

394 In this work, we some find discrepancies in the observed long-term tendencies from the utilised LTCO_3
395 products in these northern hemispheric regions. The OMI product is subject to large-scale interannual
396 variability over the 2008-17 decade, in comparison with which the underlying linear trends are small in
397 absolute terms with large confidence ranges (i.e. 95% confidence intervals) intersecting with zero. .
398 However, the OMI LTCO_3 product has been shown to be stable over this period relative to ozonesondes by
399 Pope et al., (2023). IASI-FORLI has substantial negative LTCO_3 tendencies, but this is driven by a specific
400 discontinuity in 2010 due to inhomogeneity in Eumetsat (water vapour, temperature) data used in IASI-
401 FORLI Level-2 processing (Boynard et al., 2018; Wespes et al., 2018). It induces an artificial drift that explains
402 the substantial negative LTCO_3 trends reported here and in Gaudel et al., (2018). The IASI-SOFRID LTCO_3 and
403 apriori are very similar, with little inter-annual variability, which suggests that the IASI-SOFRID O_3 retrieval in
404 this height-range is more constrained by the apriori (i.e. less TO_3 sensitivity than the other products).
405 Importantly, analysis of the three products' apriori LTCO_3 records show negligible trends meaning that year-
406 to-year sampling differences (i.e. the number of retrievals used in the spatial-monthly regional averages) are
407 not skewing long-term satellite trends. In summary: any underlying linear trend in LTCO_3 occurring during
408 the decade 2008-17 was masked by interannual variability in the OMI retrieval and by constraint to the
409 apriori in the IASI-SOFRID retrieval and, although substantial for IASI-FORLI retrieval, that is believed to be
410 due to changing meteorological input to the data processing.

411 For UKESM1.0, the model exhibits negligible temporal variability in LTCO_3 for all regions and instruments'
412 samplings. Modelled LTCO_3 trends never exceeded 1.0 DU/decade in magnitude, all of which were deemed
413 to be insignificant due to large associated p-values by the linear-seasonal trend model detailed in **Section 2.4**
414 and **Equations 4 & 5**. The ozonesondes for each region were included to ground truth the model and satellite
415 trends. The North American sites' LTCO_3 time-series was relatively noisy and exhibited considerable inter-
416 annual variability in its seasonal cycle. The comparatively low level of inter-annual variability in the European
417 UKESM1.0 record of LTCO_3 was in good agreement with the ozonesondes, however, and so was its low
418 trend, providing confidence in the model over that region. For East Asia, the interannual variability differed
419 substantially between UKESM1.0 and ozonesondes and the reported ozonesonde trend was significantly
420 much larger than for UKESM1.0. Therefore, when considering UKESM1.0 and the ozonesondes, no consistent
421 LTCO_3 trends can be determined for any of the regions. Overall, taking all data sets into account, LTO_3
422 appears to have neither increased nor decreased markedly over these three regions between the beginning
423 and end of the study decade (i.e. 2008 to 2017).

424 One key aspect of this work was to exploit UKESM1.0 to determine the importance of vertical sensitivity on
425 retrieved LTO_3 and how this influences the reported long-term tendency. In terms of the absolute model



trends (with and without the satellite AKs), the impact on LTCO_3 was small with typically near-zero tendencies and large uncertainty ranges (i.e. the 95% confidence interval). In relative terms, the changes in model trend values were more substantial in the order of 100%. To explore this further, the UKESM1.0 LTCO_3 time-series (with and without the satellite AKs) were sorted from lowest to highest (based on annual averages) to impose the most substantial trend in the model data. When the trends were re-calculated, the largest model LTCO_3 trends ranged between 0.37 and 0.90 DU/decade. When the AKs were applied, the LTCO_3 trends ranged from -0.74 to 1.02 DU/decade. Again, in relative terms, this represents a relatively large impact of the AKs on simulated LTO_3 tendencies but in absolute terms, these are small changes. Though, it should be noted that many of the 95% confidence intervals for these trends either shifted to intersect with zero or vice versa once the AKs were applied to the model. Gaudel et al., (2018) suggested two potential reasons for the TCO_3 trend discrepancies in their study:

- Time varying instrument biases/drift.
- The impact of satellite vertical sensitivity.

A further two important reasons are:

- Changes over time in latitude/longitude domains sampled by satellite sensors (e.g. GOME-1 has substantial issues after 2003).
- The time-period used for the trend analysis.

According to Boynard et al., (2018) and Wespes et al., (2018), the IASI-FORLI-v20151001 products has an artificial negative drift with time explained by a discontinuity found in the Level-2 meteorological inputs taken from Eumetsat. However, in the near future, a new consistent IASI-FORLI ozone climate data record will be available using homogeneous Level-1 and Level-2 Eumetsat meteorological data. Analysis of OMI LTCO_3 by Pope et al., 2023 showed OMI LTCO_3 to be temporally stable against ozonesondes. A similar analysis (not shown here) indicates IASI-SOFRID LTCO_3 to also be temporally stable with near-zero drift in bias. For the satellite vertical sensitivity, some of our results were unexpected. While the application of the AKs to UKESM1.0 can substantially shift the simulated absolute LTO_3 values and squash/stretch the seasonal amplitude, the impact on the simulation LTCO_3 tendencies are small in absolute terms. In relative terms, the impacts can be large (e.g. 100% change in trend rate). However, as the UKESM1.0 simulated LTCO_3 trends are generally near-zero, it is difficult to confidently say either way if the vertical sensitivity, when retrieving LTCO_3 , is important for influencing long-term tendencies, even when a more substantial trend is forced upon UKESM1.0. Future work on this would probably need to look at artificial model data which already has substantial TO_3 trends in it (e.g. 5.0 or 10.0 DU/decade). This will obviously not match reality but would provide some further quantification on how important vertical sensitivity is from different instruments/sounders in LTO_3 trend determination.

As for year-to-year sampling, our results suggest negligible trends for the product LTCO_3 apriori time-series and thus monthly sampling biases are unlikely to be introducing artificial trends as the apriori datasets are trendless. Finally, the time-period over which the trend analysis is undertaken is critically important. Gaudel et al., (2018), using the available data at the time, focussed on 2005-2015/6 and 2008-2015/6 for the OMI and IASI products they used. For the IASI products, using a slightly extended time-period, the trends show similar tendencies. However, for OMI, 2016 and 2017 represent lower years of TO_3 . As a result, this dampens the strong significant positive trends reported by Gaudel et al., (2018) in TCO_3 . It is notable that the substantial positive increase in tropical LTO_3 between 1995 and 2017 reported by Pope et al., (2023) from a series of UV-Vis sounders, included the same OMI global dataset as that is used here, further suggests the



468 selection of time period and geographical region to be crucial in regard to the role of interannual variability
469 on linear trend detection.

470 **5. Conclusions**

471 Gaudel et al., (2018) undertook a multi-satellite analysis of long-term trends in tropospheric column ozone
472 (TCO_3). They found large scale differences between these products with no clear consensus on the signs or
473 drivers of these TCO_3 trends. To avoid complications with tropopause definition and reduce influence of
474 stratospheric ozone on retrieved values, this study has undertaken a detailed follow-up assessment of
475 decadal trends in LTCO_3 (surface – 450 hPa layer) rather than TCO_3 exploiting ozonesonde records, model
476 simulations and accounting carefully for satellite O_3 metrics (e.g. averaging kernels, AKs, apriori information
477 and satellite uncertainties). We have focussed on LTCO_3 data sets from Ozone Monitoring Instrument (OMI)
478 produced by the RAL Space scheme and from Infrared Atmospheric Sounding Interferometer produced by
479 the IASI-FORLI and IASI-SOFRID schemes, for which there were consistent records from 2008-2017.

480 Evaluation of satellite LTO_3 from these three products over the North American, European and East Asian
481 regions resulted in linear trends which varied over a small range close to zero and with confidence intervals
482 intersecting with zero. This was consistent with simulations from the UK Earth System Model (UKESM1.0).
483 There were no large-scale trends in the apriori information, so changes in satellite year-to-year sampling has
484 not been driving inconsistencies between products. When convolving UKESM1.0 with the satellite AKs (i.e. to
485 assess the impact of the satellite vertical sensitivity) it did change the size of the model trend, and in some
486 instances, the direction of the trend, but as the simulated LTO_3 trends were small and insignificant, they had
487 limited influence. Overall, our results show that changes in LTO_3 during the decade 2008-2017 in North
488 America, Europe and East Asia were dominated by variability in processes which control LTO_3 on shorter
489 timescales.

490 In the future, new polar orbiting missions including the IASI Next Generation and Sentinel-5 UV/VIS sounders
491 on the MetOp Second Generation will provide tropospheric ozone products to extend current missions
492 through to the mid-2040s. There will also be the new geostationary platforms like the Infrared Sounder (IRS)
493 and Sentinel 4 UV/VIS sounder on Meteosat-Third Generation (MTG-S) and the already in orbit
494 Geostationary Environment Monitoring Spectrometer (GEMS) and Tropospheric Emissions: Monitoring of
495 Pollution (TEMPO), which will provide large volumes of data (e.g. diurnal observations) and over a long-time
496 scale on tropospheric ozone for future regional trend analyses.

497 **Acknowledgements**

498 This work was funded by the UK Natural Environment Research Council (NERC) by providing funding for the
499 National Centre for Earth Observation (NCEO, award reference NE/R016518/1) and funding from the
500 European Space Agency (ESA) Climate Change Initiative (CCI) post-doctoral fellowship scheme (award
501 reference 4000137140). For UKESM1.0 model runs, we acknowledge use of the Monsoon2 system, a
502 collaborative facility supplied under the Joint Weather and Climate Research Programme, a strategic
503 partnership between the Met Office and NERC. IASI is a joint mission of EUMETSAT and the Centre National
504 d'Etudes Spatiales (CNES, France). The IASI-SOFRID research was conducted at LAERO with some financial
505 support from the CNES French spatial agency (TOSCA–IASI project). The authors acknowledge the AERIS data
506 infrastructure for providing access to the IASI-FORLI data, ULB-LATMOS for the development of the FORLI
507 retrieval algorithm, and the AC SAF project of the EUMETSAT for providing IASI-FORLI data used in this
508 paper. Anna Maria Trofaier (ESA Climate Office) provided support and advice throughout the fellowship.

509

510



511 **Data Availability**

512 The IASI-FORLI and IASI-SOFRID data can be obtained from <https://iasi.aeris-data.fr/O3> and <https://iasi-sofrid.sedoo.fr/>. The RAL OMI data is available via the NERC Centre for Environmental Data Analysis (CEDA)
513 Jasmin platform subject to data requests. However, the RAL Space satellite data, as well as the UKESM1.0
514 simulations, will be uploaded to the Zenodo open access portal (<https://zenodo.org/>) if this manuscript is
515 accepted for publication in ACP after the peer-review process. The ozonesonde data for WOUDC, SHADOZ
516 and NOAA is available from <https://woudc.org/>, <https://tropo.gsfc.nasa.gov/shadoz/> and
517 <https://gml.noaa.gov/ozwv/ozsondes/>.

519 **Author Contributions**

520 RJP conceptualised, planned and undertook the research study. BB, ELF, BJK, RS, BGL, LJV, AB and CW
521 provided the OMI and IASI ozone data and advice on using the products. FO and MD provided advice and
522 expertise on using and running UKESM. CR provided advice and help during RP's ESA CCI fellowship. RJP
523 prepared the manuscript with scientific and technical contributions from all co-authors.

524 **Conflicts of Interest**

525 The authors declare no conflicts of interest.

526 **References:**

- 527 Archibald, A.T., O'Connor, F.M., Abraham, N.L., Archer-Nicholls, S., Chipperfield, M.P., Dalvi, M., Folberth,
528 G.A., Dennison, F., Dhomse, S.S., Griffiths, P.T., Hardacre, C., Hewitt, A.J., Hill, R.S., Johnson, C.E., Keeble, J.,
529 Kohler, M.O., Morgenstern, O., Mulcahy, J.P., Ordonez, C., Pope, R.J., Rumbold, S.T., Russo, M.R., Savage,
530 N.H., Sellar, A., Stringer, M., Turnock, S.T., Wild, O. and Zeng, G.: Description and evaluation of the UKCA
531 stratosphere–troposphere chemistry scheme (StratTrop vn 1.0) implemented in UKESM1. *Geoscientific*
532 *Model Development*, **13**, 1223–1266, doi: 10.5194/gmd-13-1223-2020, 2020.
- 533 Barret, B., Emili, E., Le Flochmoen, E. 2020. A tropopause-related climatological a priori profile for IASI-
534 SOFRID ozone retrievals: improvements and validation. *Atmospheric Measurement Techniques*, **13**, 5237–
535 5257, doi: 10.5194/amt-13-5237-2020.
- 536 Boersma, K.F., Jacob, D.J., Eskes, H.J., Pinder, R.W., Wang, J. and van der A, R.J.: Intercomparison of
537 SCIAMACHY and OMI tropospheric NO₂ columns: Observing the diurnal evolution of chemistry and emissions
538 from space. *Journal of Geophysical Research: Atmospheres*, **113** (D16S26), doi: 10.1029/2007JD008816,
539 2008.
- 540 Boersma, K. F., Eskes, H. J., Dirksen, R. J., van der A, R. J., Veefkind, J. P., Stammes, P., Huijnen, V., Kleipool,
541 Q. L., Sneep, M., Claas, J., Leitão, J., Richter, A., Zhou, Y., and Brunner, D.: An improved tropospheric
542 NO₂ column retrieval algorithm for the Ozone Monitoring Instrument, *Atmospheric Measurement*
543 *Techniques*, **4**, 1905–1928, doi: 10.5194/amt-4-1905-2011, 2011.
- 544 Boynard, A., Hurtmans, D., Garane, K., Goutail, F., Hadji-Lazaro, J., Koukouli, M. E., Wespes, C., Vigouroux, C.,
545 Keppens, A., Pommereau, J.-P., Pazmino, A., Balis, D., Loyola, D., Valks, P., Sussmann, R., Smale, D., Coheur,
546 P.-F., and Clerbaux, C.: Validation of the IASI FORLI/EUMETSAT ozone products using satellite (GOME-2),
547 ground-based (Brewer–Dobson, SAOZ, FTIR) and ozonesonde measurements, *Atmospheric Measurement*
548 *Techniques*, **11**, 5125–5152, <https://doi.org/10.5194/amt-11-5125-2018>, 2018.
- 549 Clerbaux, C., Boynard, A., Clarisse, L., George, M., Hadji-Lazaro, J., Herbin, H., Hurtmans, D., Pommier, M.,
550 Razavi, A., Turquety, S., Wespes, C. and Coheur, P.F.: Monitoring of atmospheric composition using the



- 551 thermal infrared IASI/MetOp sounder, *Atmospheric Chemistry and Physics*, 9 (16), 6041–6054,
552 doi:10.5194/acp-9-6041-2009, 2009.
- 553 Doherty, R. M., Heal, M. R., and O'Connor, F. M.: Climate change impacts on human health over Europe
554 through its effect on air quality, *Environmental Health*, 16(1), 33–44, doi:10.1186/s12940-017-0325-2, 2017.
- 555 ESA. 2019. Climate Change Initiative. <http://cci.esa.int/ozone> (last accessed 01/09/2022).
- 556 Eskes HJ and Boersma KF. 2003. Averaging kernels for DOAS total column satellite retrievals. *Atmospheric*
557 *Chemistry and Physics*, **3**, 1285–1291, doi: 10.5194/acp-3-1285-2003.
- 558 European Commission, Joint Research Centre, Dentener F, et al. 2016. Hemispheric Transport of Air Pollution
559 (HTAP): specification of the HTAP2 experiments: ensuring harmonized modelling, Publications Office,
560 <https://data.europa.eu/doi/10.2788/725244>.
- 561 Eyring, V., Bony, S., Meehl, G. A., Senior, C. A., Stevens, B., Stouffer, R. J., and Taylor, K. E.: Overview of the
562 Coupled Model Intercomparison Project Phase 6 (CMIP6) experimental design and organization, *Geosci.*
563 *Model Dev.*, 9, 1937–1958, <https://doi.org/10.5194/gmd-9-1937-2016>, 2016. Gaudel A, et al. 2018.
564 Tropospheric Ozone Assessment Report: Present day distribution and trends of tropospheric ozone relevant
565 to climate and global atmospheric chemistry model evaluation. *Elementa*, **6 (39)**, 1-58, doi:
566 10.1525/elementa.291.
- 567 Forster, P., Storelvmo, T., Armour, K., Collins, W., Dufresne, J.-L., Frame, D., Lunt, D. J., Mauritsen, T.,
568 Palmer, M. D., Watanabe, M., Wild, M., and Zhang, H.: The Earth's Energy Budget, Climate Feedbacks, and
569 Climate Sensitivity, in: *Climate Change 2021: The Physical Science Basis*, Contribution of Working Group I to
570 the Sixth Assessment Report of the Intergovernmental Panel on Climate Change, edited by: Masson-
571 Delmotte, V., Zhai, P., Pirani, A., Connors, S. L., Péan, C., Berger, S., Caud, N., Chen, Y., Goldfarb, L., Gomis, M.
572 I., Huang, M., Leitzell, K., Lonnoy, E., Matthews, J. B. R., Maycock, T. K., Waterfield, T., Yelekçi, O., Yu, R., and
573 Zhou, B., Cambridge University Press, Cambridge, United Kingdom and New York, NY, USA, 923–1054,
574 doi:10.1017/9781009157896.009, 2021.
- 575 Gaudel, A., Cooper, O.R., Ancellet, G., Barret, B., Boynard, A., Burrows, J.P., Clerbaux, C., Coheur, P.F.,
576 Cuesta, J., Cuevas, E., Doniki, S., Dufour, G., Ebojio, F., Foret, G., Garia, O., Granados-Munoz, M.J., Hannigan,
577 J.W., Hase, F., Hassler, B., Huang, G., Hurtmans, D., Jaffe, D., Jones, N., Kalabokas, P., Kerridge, B., Kulwaik, S.,
578 Latter, B., Leblanc, T., Le Flochmoen, E., Lin, W., Liu, J., Liu, X., Mahieu, E., McClure-Begley, A., Neu, J.L.,
579 Osman, M., Palm, M., Petetin, H., Petropavlovskikh, I., Querel, R., Rahpoe, N., Rozanov, A., Schultz, M.G.,
580 Schwab, J., Siddans, R., Smale, D., Steinbacher, M., Tanimoto, H., Tarasick, D.W., Thouret, V., Thompson,
581 A.M., Trickl, T., Weatherhead, E., Wespes, C., Worden, H.M., Vigouroux, C., Xu, X., Zeng, G. and Ziemke, J.:
582 Tropospheric Ozone Assessment Report: Present day distribution and trends of tropospheric ozone relevant
583 to climate and global atmospheric chemistry model evaluation. *Elementa*, **6(39)**, 1-58,
584 doi:10.1525/elementa.291, 2018.
- 585 Gauss, M., Myhre, G., Isaksen, I. S. A., Grewe, V., Pitari, G., Wild, O., Collins, W. J., Dentener, F. J., Ellingsen,
586 K., Gohar, L. K., Hauglustaine, D. A., Iachetti, D., Lamarque, F., Mancini, E., Mickley, L. J., Prather, M. J., Pyle,
587 J. A., Sanderson, M. G., Shine, K. P., Stevenson, D. S., Sudo, K., Szopa, S., and Zeng, G.: Radiative forcing since
588 preindustrial times due to ozone change in the troposphere and the lower stratosphere, *Atmospheric*
589 *Chemistry and Physics*, **6**, 575–599, <https://doi.org/10.5194/acp-6-575-2006>, 2006.
- 590 Hoesly, R. M., Smith, S. J., Feng, L., Klimont, Z., Janssens-Maenhout, G., Pitkanen, T., Seibert, J. J., Vu, L.,
591 Andres, R. J., Bolt, R. M., Bond, T. C., Dawidowski, L., Kholod, N., Kurokawa, J.-I., Li, M., Liu, L., Lu, Z., Moura,



- 592 M. C. P., O'Rourke, P. R., and Zhang, Q.: Historical (1750–2014) anthropogenic emissions of reactive gases
593 and aerosols from the Community Emissions Data System (CEDS), *Geoscientific Model Development*, 11,
594 369–408, <https://doi.org/10.5194/gmd-11-369-2018>, 2018.
- 595 Hollaway, M.J., Arnold, S.R., Challinor, A. J. and Emberson, L.D: Intercontinental trans-boundary
596 contributions to ozone-induced crop yield losses in the North Hemisphere, *Biogeosciences*, 9, 271–2929, doi:
597 10.5194/bg-9-271-2012, 2012.
- 598 Illingworth, S. M., Remedios, J. J., Boesch, H., Moore, D. P., Sembhi, H., Dudhia, A., and Walker, J. C.: ULIRS,
599 an optimal estimation retrieval scheme for carbon monoxide using IASI spectral radiances: sensitivity
600 analysis, error budget and simulations, *Atmospheric Measurements Techniques*, 4, 269–288, doi:
601 10.5194/amt-4-269-2011, 2011.
- 602 Keim, C., Eremenko, M., Orphal, J., Dufour, G., Flaud, J.-M., Höpfner, M., Boynard, A., Clerbaux, C., Payan, S.,
603 Coheur, P.-F., Hurtmans, D., Claude, H., Dier, H., Johnson, B., Kelder, H., Kivi, R., Koide, T., López Bartolomé,
604 M., Lambkin, K., Moore, D., Schmidlin, F. J., and Stübi, R.: Tropospheric ozone from IASI: comparison of
605 different inversion algorithms and validation with ozone sondes in the northern middle latitudes,
606 *Atmospheric Chemistry and Physics*, 9, 9329–9347, doi: 10.5194/acp-9-9329-2009, 2009.
- 607 Lamarque, J.-F., Bond, T. C., Eyring, V., Granier, C., Heil, A., Klimont, Z., Lee, D., Liousse, C., Mieville, A.,
608 Owen, B., Schultz, M. G., Shindell, D., Smith, S. J., Stehfest, E., Van Aardenne, J., Cooper, O. R., Kainuma, M.,
609 Mahowald, N., McConnell, J. R., Naik, V., Riahi, K., and van Vuuren, D. P.: Historical (1850–2000) gridded
610 anthropogenic and biomass burning emissions of reactive gases and aerosols: methodology and application,
611 *Atmospheric Chemistry and Physics*, 10, 7017–7039, doi: 10.5194/acp-10-7017-2010, 2010.
- 612 Matthes, K., Funke, B., Andersson, M. E., Barnard, L., Beer, J., Charbonneau, P., Clilverd, M. A., Dudok de Wit,
613 T., Haberreiter, M., Hendry, A., Jackman, C. H., Kretschmar, M., Kruschke, T., Kunze, M., Langematz, U.,
614 Marsh, D. R., Maycock, A. C., Misios, S., Rodger, C. J., Scaife, A. A., Seppälä, A., Shangguan, M., Sinnhuber,
615 M., Tourpali, K., Usoskin, I., van de Kamp, M., Verronen, P. T., and Versick, S.: Solar forcing for CMIP6 (v3.2),
616 *Geoscientific Model Development*, 10, 2247–2302, <https://doi.org/10.5194/gmd-10-2247-2017>, 2017.
- 617 McPeters, R.D., Labow, G.J., and Logan, J.A. 2007. Ozone climatological profiles for satellite retrieval
618 algorithms. *Journal of Geophysical Research*, 112 (D05308), <https://doi.org/10.1029/2005JD006823>.
- 619 Miles, G.M., Siddans, R., Kerridge, B. J., Latter, B. G., and Richards, N. A. D.: Tropospheric ozone and ozone
620 profiles retrieved from GOME-2 and their validation, *Atmospheric Measurement Techniques*, 8, 385–398,
621 doi:10.5194/amt-8-385-2015, 2015.
- 622 Monks, S.A., Arnold, S.R., Hollaway, M. J., Pope, R.J., Wilson, C., Feng, W., Emmerson, K.E., Kerridge, B.J.,
623 Latter, B.L., Miles, G.M., Siddans, R. and Chipperfield, M.P.: The TOMCAT global chemistry transport model
624 v1.6: Description of chemical mechanism and model evaluation, *Geoscientific Model Development*, 10 (8),
625 3025–3057, doi:10.5194/gmd-10-3025-2017, 2017.
- 626 Myhre, G., Shindell, D., Bréon, F.-M., Collins, W., Fuglestad, J., Huang, J., Koch, D., Lamarque, J.-F., Lee, D.,
627 Mendoza, B., Nakajima, T., Robock, A., Stephens, G., Takemura, T. and Zhang, H.: Anthropogenic and Natural
628 Radiative Forcing, in: Climate Change 2013: The Physical Science Basis. Contribution of Working Group I to
629 the Fifth Assessment Report of the Intergovernmental Panel on Climate Change, Cambridge University Press,
630 Cambridge, United Kingdom and New York, NY, USA, 659–740, 2013.
- 631 O'Connor, F. M., Johnson, C. E., Morgenstern, O., Abraham, N. L., Braesicke, P., Dalvi, M., Folberth, G. A.,
632 Sanderson, M. G., Telford, P. J., Voulgarakis, A., Young, P. J., Zeng, G., Collins, W. J., and Pyle, J. A.: Evaluation



- of the new UKCA climate-composition model – Part 2: The Troposphere, *Geoscientific Model Development*,
7, 41–91, doi: 10.5194/gmd-7-41-2014, 2014.
- Pimlott, M.A., Pope, R.P., Kerridge, B.J., Latter, B.G., Knappett, D.S., Heard, D.E., Ventress, L.J., Siddans, R.,
Feng, W. and Chipperfield, M.P.: Investigating the global OH radical distribution using steady-state
approximations and satellite data. *Atmospheric Chemistry and Physics*, **22**, 10467–10488, doi: 10.5194/acp-
22-10467-2022, 2022.
- Pope, R.J., Arnold, S.R., Chipperfield, M.P., Latter, B.G., Siddans, R. and Kerridge, B.J.: Widespread changes in
UK air quality observed from space. *Atmospheric Science Letters*, **19**:e817, doi: 10.1002/asl.817.
- Pope, R. J., Kerridge, B. J., Siddans, R., Latter, B. G., Chipperfield, M. P., Feng, W., Pimlott, M. A., Dhomse, S.
S., Retscher, C., and Rigby, R.: Investigation of spatial and temporal variability in lower tropospheric ozone
from RAL Space UV–Vis satellite products, *Atmospheric Chemistry and Physics*, **23**, 14933–14947,
<https://doi.org/10.5194/acp-23-14933-2023>, 2023.
- Rao, S., Klimont, Z., Smith, S.J., Van Dingenen, R., Dentener, F., Bouwman, L., Riahi, K., Amann, M., Bodirsky,
B.L., van Vuuren, D.P., Reus, L.R., Calvin, K., Drouet, L., Fricko, O., Fujimori, S., Gernaat, D., Havlik, P.,
Harmesen, M., Hasegawa, T., Heyes, C. and Tavoni, M.: Future air pollution in the shared socio-economic
pathways. *Global Environmental Change*, **42**, 346–358, doi: 10.1016/j.gloenvcha.2016.05.012.
- Richards, N.A.D, Osterman, G.B., Browell, E.V., Hair, J.W., Avery, M. and Li, Q.: Validation of tropospheric
emission spectrometer ozone profiles with aircraft observations during the intercontinental chemical
transport experiment–B. *Journal Geophysical Research*, **113**(D16S29), doi: 10.1029/2007JD008815, 2008.
- Sellar, A.A., Jones, C.G., Mulcahy, J.P., Tang, Y., Yool, A., Wiltshire, A., O’Connor, F.M., Stringer, M., Hill, R.,
Palmieri, J., Woodward, S., de Mora, L., Kuhlbrodt, T., Rumbold, S.T., Kelley, D.I., Ellis, R., John, C.E., Walton,
J., Abraham, N.L., Andrews, M.B., Andrews, T., Archibald, A.T., Berthou, S., Burke, E., Blockley, E., Carslaw, K.,
Dalvi, M., Edwards, J., Folbert, G.A., Gedney, N., Griffiths, P.T., Harper, A.B., Hendry, M.A., Hewitt, A.J.,
Johnson, B., Jones, A., Jones, C.D., Keebie, J., Liddicoat, S., Morgenstern, O., Parker, R.J., Predoi, V.,
Robertson, E., Siahann, A., Smith, R.S., Swaminathan, R., Woodhouse, M.T., Zeng, G. and Zerroukat, M.:
Description and Evaluation of the UK Earth System Model. *Journal of Advances in Modeling Earth Systems*,
11, 4513–4558, doi: 10.1029/2019MS001739, 2019.
- Sindelarova, K., Granier, C., Bouarar, I., Guenther, A., Tilmes, S., Stavrakou, T., Müller, J.-F., Kuhn, U., Stefani,
P., and Knorr, W.: Global data set of biogenic VOC emissions calculated by the MEGAN model over the last
30 years, *Atmos. Chem. Phys.*, **14**, 9317–9341, doi: 10.5194/acp-14-9317-2014, 2014.
- Sitch, S., Cox, P.M., Collins, W.J., & Huntingford, C.: Indirect radiative forcing of climate change through
ozone effects on the land carbon sink, *Nature*, **448**, 791–795, doi:10.1038/nature06059, 2007.
- Telford, P. J., Braesicke, P., Morgenstern, O., and Pyle, J. A.: Technical Note: Description and assessment of a
nudged version of the new dynamics Unified Model, *Atmospheric Chemistry and Physics*, **8**, 1701–1712,
<https://doi.org/10.5194/acp-8-1701-2008>, 2008.
- van der A, R.J., Peters, D.H.M.U., Eskes, H., Boersma, K.F., Van Roozendaal, M., De Smedt, I. and Kelder,
H.M.: Detection of the trend and seasonal variation in tropospheric NO₂ over China. *Journal of Geophysical
Research*, **11**, D12317, doi: 10.1029/2005JD006594, 2006.
- van der A, R.J., Eskes, H.J., Boersma, K.F., van Noije, T.P.C., Van Roozendaal, M., De Smedt, I., Peters,
D.H.M.U. and Meijer, E.W.: Trends, seasonal variability and dominant NO_x sources derived from a ten year



- 673 record of NO₂ measured from space. *Journal of Geophysical Research*, **113**, 1–12, doi:
674 10.1029/2007JD009021, 2008.
- 675 van der Werf, G. R., Randerson, J. T., Giglio, L., van Leeuwen, T. T., Chen, Y., Rogers, B. M., Mu, M., van
676 Marle, M. J. E., Morton, D. C., Collatz, G. J., Yokelson, R. J., and Kasibhatla, P. S.: Global fire emissions
677 estimates during 1997–2016, *Earth System Science Data*, 9, 697–720, [https://doi.org/10.5194/essd-9-697-](https://doi.org/10.5194/essd-9-697-2017)
678 2017, 2017.
- 679 van Marle, M. J. E., Kloster, S., Magi, B. I., Marlon, J. R., Daniau, A.-L., Field, R. D., Arneeth, A., Forrest, M.,
680 Hantson, S., Kehrwald, N. M., Knorr, W., Lasslop, G., Li, F., Mangeon, S., Yue, C., Kaiser, J. W., and van der
681 Werf, G. R.: Historic global biomass burning emissions for CMIP6 (BB4CMIP) based on merging satellite
682 observations with proxies and fire models (1750–2015), *Geoscientific Model Development*, 10, 3329–3357,
683 <https://doi.org/10.5194/gmd-10-3329-2017>, 2017.
- 684 Weatherhead, E.C., Reinsel, G.C., Tiao, G.C., Meng, X., Choi, D., Cheang, W., Keller, T., De Luisi, J., Wuebbles,
685 D.J., Kerr, J.B., Miller, A.J., Oltmans, S.J. and Frederick, J.E.: Factors affecting the detection of trends:
686 statistical considerations and applications to environmental data. *Journal of Geophysical Research*, **103(D14)**,
687 17149–17161, doi: 10.1029/98JD00995, 1998.
- 688 Wespes, C., Hurtmans, D., Clerbaux, C., Boynard, A., and Coheur, P.-F. 2018. Decrease in tropospheric O₃
689 levels in the Northern Hemisphere observed by IASI. *Atmospheric Chemistry and Physics*, **18**, 6867–6885,
690 doi:10.5194/acp-18-6867-2018.
- 691 WHO (World Health Organisation), Ambient (outdoor) air pollution, available at: [https://www.who.int/news-](https://www.who.int/news-room/fact-sheets/detail/ambient-(outdoor)-air-quality-and-health)
692 room/fact-sheets/detail/ambient-(outdoor)-air-quality-and-health (last accessed 2nd January 2024), 2022.
- 693 Wiltshire, A.J., Burke, E.J., Chadburn, S.E., Jones, C.D., Cox, P.M., Davies-Barnard, T., Friedlingstein, P.,
694 Harper, A.B., Liddicoat, S., Sitch, S. and Zaehle, S.: JULES-CN: a coupled terrestrial carbon–nitrogen scheme
695 (JULES vn5.1). *Geophysical Model Development*, 14 (4), 2161–2186, doi: 10.5194/gmd-14-2161-2021,
696 2021.Yool A, et al. 2013. MEDUSA-2.0: an intermediate complexity biogeochemical model of the marine
697 carbon cycle for climate change and ocean acidification studies. *Geoscientific Model Development*, **6**, 1767–
698 1811, doi: 10.5194/gmd-6-1767-2013.
- 699 Young, P.J., Archibald, A.T., Bowman, K.W., Lamarque, J.-F., Naik, V., Stevenson, D.S., Tilmes, S., Voulgarakis,
700 A., Wild, O., Bergmann, D., Cameron-Smith, P., Cionni, I., Collins, W.J., Dalsoren, S.B., Doherty, R.M., Eyring,
701 V., Faluvegi, G., Horowitz, L.W., Josse, B., Lee, Y.H., MacKenzie, I.A., Nagashima, T., Plummer, D.A., Righi, M.,
702 Rumbold, S.T., Skeie, R.B., Shindell, D.T., Strode, S.A., Sudo, K., Szopa, S. and Zeng, G.: Pre-industrial to end
703 21st century projections of tropospheric ozone from the Atmospheric Chemistry and Climate Model
704 Intercomparison Project (ACCMIP). *Atmospheric Chemistry and Physics*, 13, 2063–2090, doi: 10.5194/acp-13-
705 2063-2013, 2013.
- 706 Ziemke, J.R., Chandra, S., Labow, G.J., Bhartia, P.K., Froidevaux, L. and Witte, J.C.: A global climatology of
707 tropospheric and stratospheric ozone derived from Aura OMI/MLS measurements, *Atmospheric Chemistry*
708 *and Physics*, 11, 9237–9251, doi: /10.5194/acp-11-9237-2011, 2011.

709
710
711
712



Figures & Tables:

713

714

Data Provider	Satellite Profile Products & Version	Product Link	Data Range	Data Size
RAL Space	OMI-fv214	http://www.ceda.ac.uk/	2004-2018	1442 GB
ATMOS-ULB	IAS-FORLI-v20151001	https://iasi.aeris-data.fr/catalog/	2008-2019	9.1 TB
Université de Toulouse	IASI-SOFRID vn3.5	https://iasi-sofrid.sedoo.fr/	2008-2017	3.0 TB

715

Table 1: List of the satellite ozone profile data sets.

716

717

Satellite	Quantity	Trend	Trend Lower	Trend Upper	p-value	Fit (R ²)
OMI	Trend	-0.79	-7.07	5.48	0.80	0.58
	Trend Error 1	-1.50	-7.04	4.04	0.59	0.68
	Trend Error 2	-0.09	-6.98	6.81	0.98	0.50
	Apriori Trend	-0.05	-0.21	0.11	0.56	1.00
	UKESM Trend	0.21	-0.37	0.78	0.47	0.95
	UKESM+AKs Trend	-0.57	-1.58	0.45	0.26	0.90
	UKESM Trend Forced	0.73	0.22	1.25	0.00	0.95
	UKESM+AKs Trend Forced	-0.74	-1.89	0.40	0.20	0.89
FORLI	Trend	-1.42	-2.35	-0.50	0.00	0.93
	Trend Error 1	-1.34	-2.21	-0.47	0.00	0.93
	Trend Error 2	-1.50	-2.51	-0.50	0.00	0.93
	Apriori Trend	0.00	-0.11	0.12	0.94	0.67
	UKESM Trend	-0.13	-0.75	0.49	0.67	0.93
	UKESM+AKs Trend	-0.32	-0.83	0.20	0.22	0.92
	UKESM Trend Forced	0.64	-3.50	4.77	0.76	0.46
	UKESM+AKs Trend Forced	0.55	0.08	1.03	0.02	0.93
SOFRID	Trend	0.12	-0.59	0.82	0.74	0.94
	Trend Error 1	0.14	-0.59	0.88	0.70	0.90
	Trend Error 2	0.09	-0.48	0.66	0.75	0.94
	Apriori Trend	0.11	-0.17	0.39	0.43	0.98
	UKESM Trend	-0.24	-0.85	0.37	0.44	0.95
	UKESM+AKs Trend	-0.04	-0.53	0.45	0.87	0.97
	UKESM Trend Forced	0.80	0.41	1.19	0.00	0.97
	UKESM+AKs Trend Forced	0.58	0.24	0.92	0.00	0.98
OMI	Trend	-0.80	-7.29	5.69	0.80	0.71
	Trend Error 1	-1.65	-6.92	3.62	0.53	0.76
	Trend Error 2	0.05	-7.44	7.53	0.99	0.67
	Apriori Trend	-0.12	-0.26	0.03	0.10	1.00
	UKESM Trend	-0.11	-0.50	0.29	0.59	0.99
	UKESM+AKs Trend	-0.72	-1.77	0.32	0.16	0.95
	UKESM Trend Forced	0.62	0.14	1.10	0.01	0.98
	UKESM+AKs Trend Forced	0.47	-0.51	1.44	0.34	0.94



FORLI	Trend	-1.83	-2.78	-0.89	0.00	0.92
	Trend Error 1	-1.80	-2.72	-0.88	0.00	0.93
	Trend Error 2	-1.87	-2.87	-0.87	0.00	0.92
	Apriori Trend	0.09	-0.09	0.27	0.32	0.48
	UKESM Trend	-0.28	-0.77	0.20	0.25	0.98
	UKESM+AKs Trend	-0.43	-1.21	0.35	0.27	0.94
	UKESM Trend Forced	0.37	-0.05	0.79	0.08	0.98
	UKESM+AKs Trend Forced	0.28	-0.38	0.94	0.40	0.93
SOFRIID	Trend	0.05	-0.91	1.01	0.92	0.93
	Trend Error 1	0.16	-0.74	1.07	0.72	0.91
	Trend Error 2	-0.07	-0.91	0.78	0.87	0.93
	Apriori Trend	0.17	-0.12	0.45	0.24	0.98
	UKESM Trend	-0.27	-0.72	0.19	0.24	0.98
	UKESM+AKs Trend	0.08	-0.33	0.49	0.69	0.98
	UKESM Trend Forced	0.46	0.09	0.84	0.01	0.99
	UKESM+AKs Trend Forced	0.10	-0.32	0.51	0.64	0.98
OMI	Trend	-0.09	-7.88	7.70	0.98	0.51
	Trend Error 1	-1.05	-6.61	4.52	0.70	0.66
	Trend Error 2	0.87	-8.24	9.98	0.85	0.38
	Apriori Trend	-0.25	-0.71	0.22	0.29	0.98
	UKESM Trend	-0.16	-0.94	0.62	0.67	0.98
	UKESM+AKs Trend	-0.62	-2.24	1.00	0.44	0.95
	UKESM Trend Forced	0.90	0.34	1.47	0.00	0.99
	UKESM+AKs Trend Forced	1.02	-0.04	2.09	0.05	0.97
FORLI	Trend	-1.52	-2.16	-0.88	0.00	0.93
	Trend Error 1	-1.42	-2.06	-0.78	0.00	0.93
	Trend Error 2	-1.62	-2.27	-0.98	0.00	0.92
	Apriori Trend	-0.03	-0.22	0.16	0.76	0.21
	UKESM Trend	-0.03	-0.62	0.56	0.93	0.98
	UKESM+AKs Trend	-0.29	-0.80	0.22	0.25	0.95
	UKESM Trend Forced	0.66	0.15	1.17	0.01	0.98
	UKESM+AKs Trend Forced	0.08	-0.44	0.61	0.75	0.93
SOFRIID	Trend	-0.19	-1.01	0.63	0.65	0.96
	Trend Error 1	-0.08	-0.73	0.58	0.82	0.90
	Trend Error 2	-0.30	-1.02	0.42	0.41	0.93
	Apriori Trend	-0.15	-0.39	0.09	0.21	0.98
	UKESM Trend	-0.42	-0.97	0.13	0.12	0.99
	UKESM+AKs Trend	-0.24	-0.67	0.20	0.28	0.98
	UKESM Trend Forced	0.63	0.26	1.00	0.00	0.99
	UKESM+AKs Trend Forced	0.20	-0.20	0.61	0.31	0.98

718

719 **Table 2:** LTCO₃ trends (DU/decade) for the satellite trend (Trend), the satellite-uncertainty trend (Trend Error

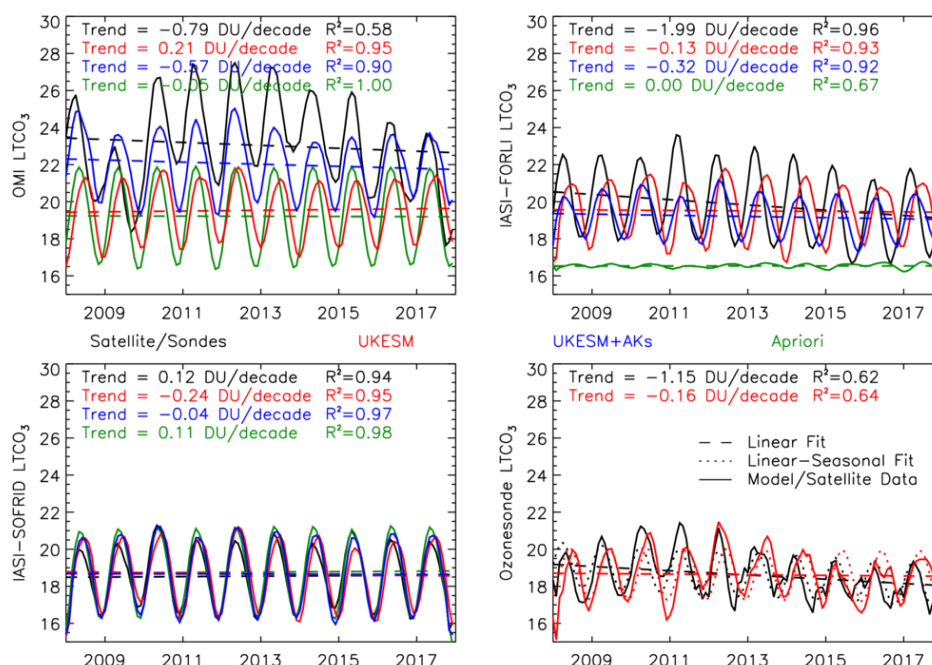
720 1), the satellite+uncertainty trend (Trend Error 2), the satellite apriori trend (Apriori Trend), UKESM trend

721 (UKESM Trend), UKESM with AKs applied trend (UKESM+AKs Trend), UKESM forced trend (UKESM Trend

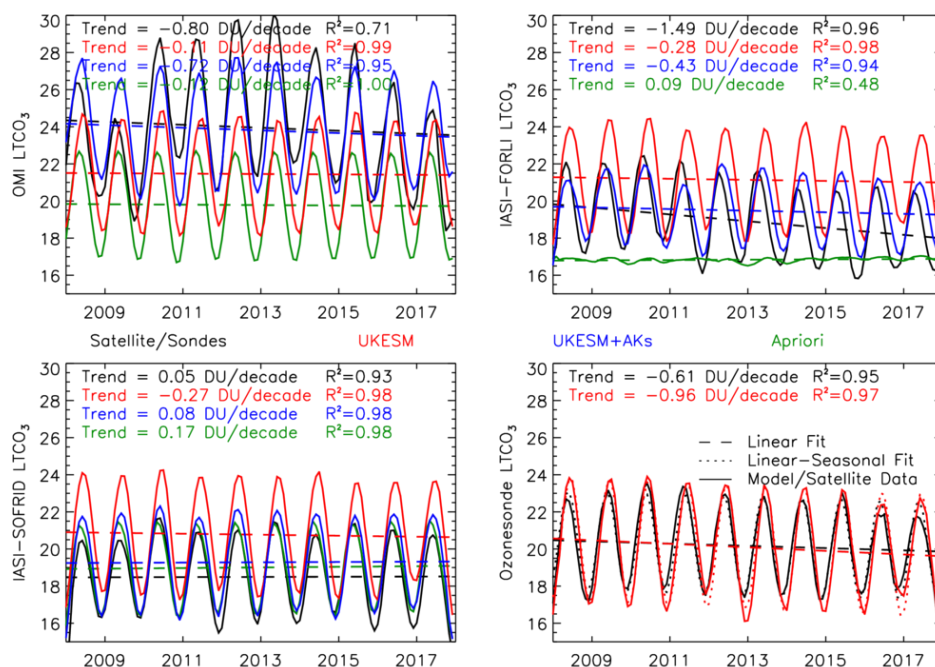
722 Forced) and UKESM with AKs applied forced trend (UKESM+AKs Trend Forced). The trends from OMI, IASI-



723 FORLI and IASI-SOFRID are for North America (red), Europe (blue) and East Asia (green). The trend lower and
724 trend upper represent the trend 95% confidence interval. R^2 is the trend fit skill (i.e. correlation squared) and
725 the p -value is also shown.
726
727

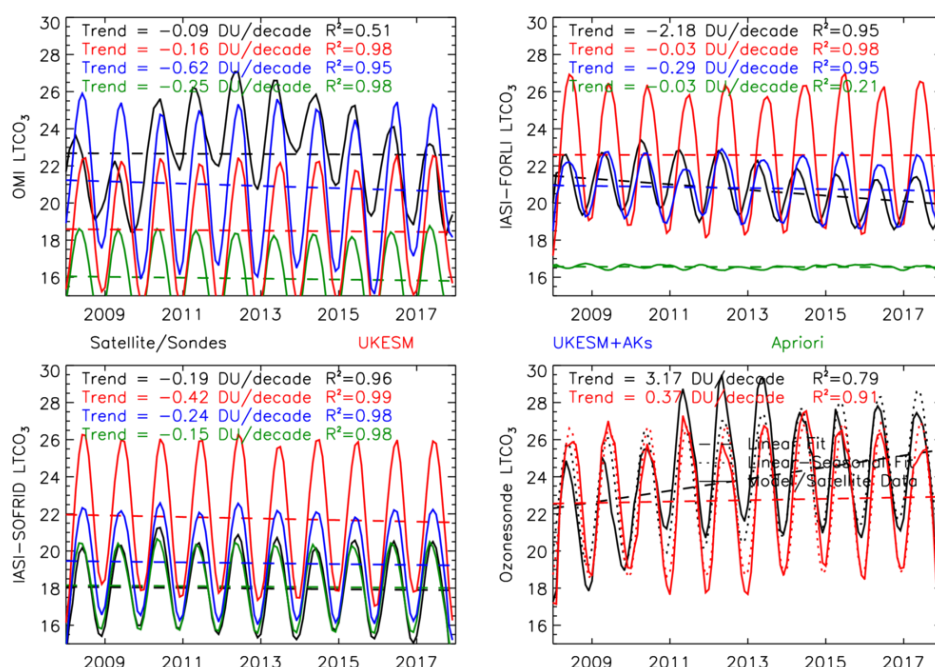


728
729 **Figure 1:** Lower tropospheric column ozone ($LTCO_3$, surface to 450 hPa, DU) regional time-series for North
730 America, based on the HTAP land mask, from OMI (top-left), IASI-FORLI (top-right), IASI-SOFRID (bottom-left)
731 and ozonesondes (bottom-right) are shown by the black lines in the respective panels. UKESM simulations
732 without and with satellite averaging kernels (AKs) applied are shown in red and blue lines. Green lines show
733 the satellite apriori. Dashed lines show the $LTCO_3$ linear trend which are labelled in the top of each panel. The
734 R^2 squared values show the linear-seasonal trend model fit to the corresponding $LTCO_3$ time-series (i.e.
735 correlation squared).



736

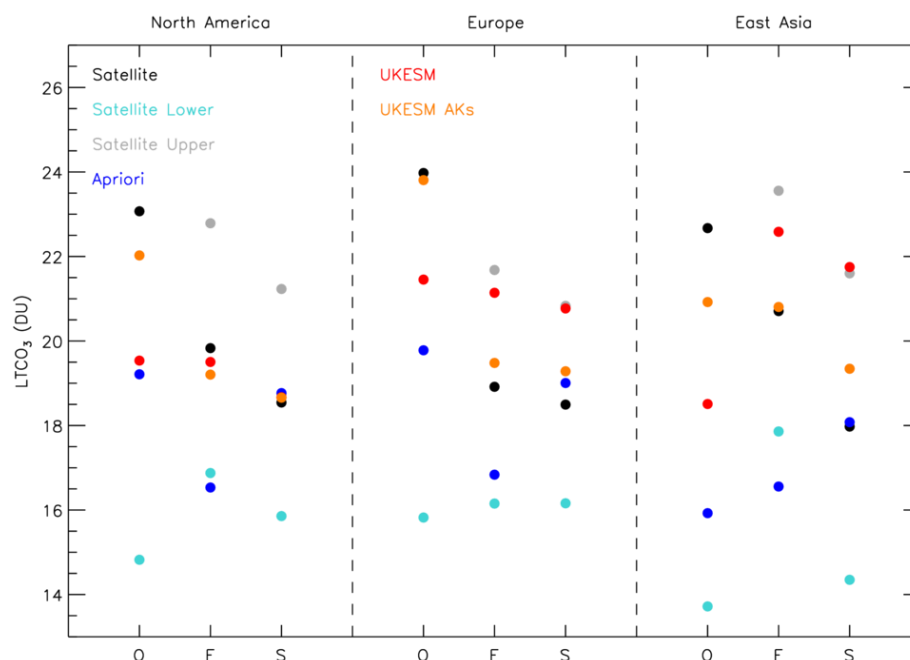
737 **Figure 2:** LTCO₃ (DU) regional time-series for Europe, based on the HTAP land mask, from OMI (top-left), IASI-
738 FORLI (top-right), IASI-SOFRID (bottom-left) and ozonesondes (bottom-right) are shown by the black lines in
739 the respective panels. UKESM simulations without and with satellite AKs applied are shown in red and blue
740 lines. Green lines show the satellite apriori. Dashed lines show the LTCO₃ linear trend which are labelled in the
741 top of each. The R² squared values show the linear-seasonal trend model fit to the corresponding LTCO₃ time-
742 series (i.e. correlation squared).



743

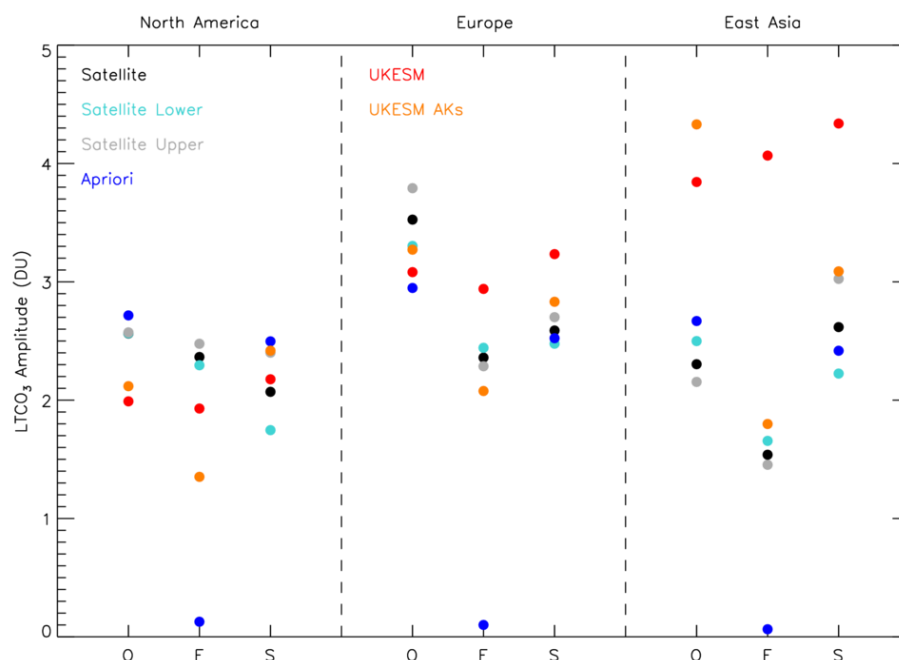
744 **Figure 3:** LTCO_3 (DU) regional time-series for East Asia, based on the HTAP land mask, from OMI (top-left),
745 IASI-FORLI (top-right), IASI-SOFRID (bottom-left) and ozonesondes (bottom-right) are shown by the black lines
746 in the respective panels.. UKESM simulations without and with satellite AKs applied are shown in red and blue
747 lines. Green lines show the satellite apriori. Dashed lines show the LTCO_3 linear trend which are labelled in the
748 top of each panel. The R^2 squared values show the linear-seasonal trend model fit to the corresponding LTCO_3
749 time-series (i.e. correlation squared).

750



751

752 **Figure 4:** Average $LT\text{CO}_3$ (DU) values across the 2008-2017 time-period for the satellite (black), satellite-lower
753 (cyan), satellite-upper (grey), apriori (blue), UKESM (red) and UKESM+AKs (orange). The satellite-lower and
754 satellite-upper values are the average of the satellite \pm its error term time-series (note: these values do not
755 always fit in the y-axis range). O, F and S represent OMI, IASI-FORLI and IASI-SOFRID for North America (left),
756 Europe (centre) and East Asia (right).



757

758 **Figure 5:** Average LTCO_3 seasonal cycle amplitude (DU) values across the 2008-2017 time-period for the
759 satellite (black), satellite-lower (cyan), satellite-upper (grey), apriori (blue), UKESM (red) and UKESM+AKs
760 (orange). The satellite-lower and satellite-upper values are the average of the satellite \pm its error term time-
761 series (note: these values do not always fit in the y-axis range). O, F and S represent OMI, IASI-FORLI and IASI-
762 SOFRID for North America (left), Europe (centre) and East Asia (right).

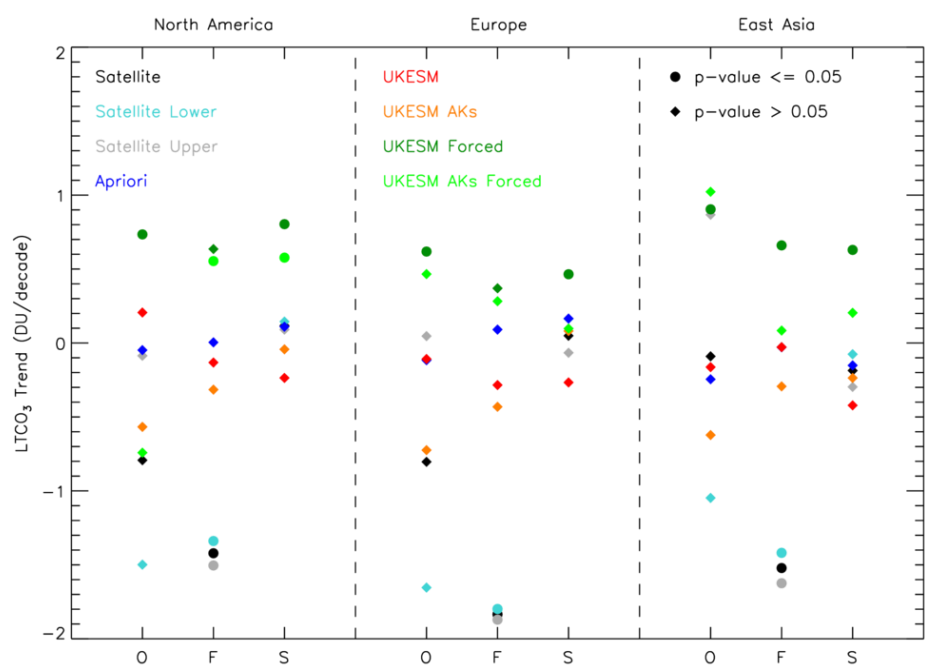


Figure 6: Average LTCO_3 linear trends (DU/decade) values across the 2008-2017 time-period for the satellite (black), satellite-lower (cyan), satellite-upper (grey), apriori (blue), UKESM (red), UKESM+AKs (orange), UKESM forced (dark green) and UKESM+AKs forced (light green). The satellite-lower and satellite-upper values are the average of the satellite \pm its error term time-series (note: these values do not always fit in the y-axis range). O, F and S represent OMI, IASI-FORLI and IASI-SOFRID for North America (left), Europe (centre) and East Asia (right). Triangle and circular symbols represent linear trends with p -values > 0.05 or $p \leq 0.05$, respectively.